

Strain Monitoring using a Rayleigh Backscattering System for a Composite UAV Wing Instrumented with an Embedded Optical Fiber

Martinez Bueno, Patricia; Martinez, Marcias; Rans, Calvin; Benedictus, Rinze

DOI

[10.4028/www.scientific.net/AMR.1135.1](https://doi.org/10.4028/www.scientific.net/AMR.1135.1)

Publication date

2016

Document Version

Accepted author manuscript

Published in

Advanced Materials Research

Citation (APA)

Martinez Bueno, P., Martinez, M., Rans, C., & Benedictus, R. (2016). Strain Monitoring using a Rayleigh Backscattering System for a Composite UAV Wing Instrumented with an Embedded Optical Fiber. *Advanced Materials Research*, 1135, 1-19. <https://doi.org/10.4028/www.scientific.net/AMR.1135.1>

Important note

To cite this publication, please use the final published version (if applicable). Please check the document version above.

Copyright

Other than for strictly personal use, it is not permitted to download, forward or distribute the text or part of it, without the consent of the author(s) and/or copyright holder(s), unless the work is under an open content license such as Creative Commons.

Takedown policy

Please contact us and provide details if you believe this document breaches copyrights. We will remove access to the work immediately and investigate your claim.

Strain Monitoring using a Rayleigh Backscattering System for a Composite UAV Wing Instrumented with an Embedded Optical Fiber

Patricia Martinez Bueno^{1,2,a}, Marcias Martinez^{3,1,b,*}, Calvin Rans^{1,c},
Rinze Benedictus^{1,d}

¹ Faculty of Aerospace Engineering, Delft University of Technology, Delft, Building 62, Kluyverweg 1, 2629HS Delft, P.O. Box 5058, 2600 GB Delft, The Netherlands

² Escuela Superior de Ingenieros Aeronáuticos, Universidad Politécnica de Madrid, Madrid, Pza. Cardenal Cisneros 3, Madrid, 28040, Spain

³ Clarkson University, Department of Mechanical and Aeronautical Engineering, Potsdam, N.Y., 13699, USA

^a patricia.mbueno@alumnos.upm.es, ^{b,*} mmartine@clarkson.edu, ^c C.D.Rans@tudelft.nl,
^d R.Benedictus@tudelft.nl

Keywords: Rayleigh Backscattering, Embedded Optical Fiber, Unmanned Aerial Vehicles, Strain Monitoring, Composite Wing, Distributed Sensing System.

Abstract. The primary objective of this research study was to evaluate the capabilities for measuring strain of a composite UAV wing with an embedded optical fiber connected to a Rayleigh backscattering distributed sensing system. This research paper summarizes the manufacturing procedure used during the instrumentation of the composite UAV wing. In addition, a Finite Element Model was developed in order to verify the strain distribution of this complex structure under static and dynamic loading conditions. The use of strain gauge data as a means for verification is presented as part of this research. Finally, fatigue tests were carried out to determine the longevity of the embedded fiber during the design life of the structure. The results demonstrate the ability of a distributed sensing system to obtain complex and accurate strain distributions on a single non-grated fiber. In addition, the findings demonstrate current limitations of the system for capturing accurate strain profiles in dynamic loading test cases.

Introduction

The presence of Fiber Reinforced Polymer (FRP) composites has steadily grown within the aerospace industry. The use of composites materials has progressively increased from non-critical secondary structures into primary airframe structures. One of the advantages driving the increased use of composites is their specific strength and stiffness, which translates into a reduction in weight while maintaining or improving the structural performance of the aircraft. Despite these advancements, there is still a lack of experience on the loading behavior and damage evolution in composites when compared to their metallic counterparts. To combat this uncertainty, higher design safety factors and/or increased operational inspections are typically employed to ensure adequate safety [1].

A key enabler in increasing the understanding, and thus safety, regarding the behavior and failure of composite structures is the ability to determine the precise loading/strain within a particular structure. The nature of composite materials and their fabrication can introduce manufacturing anomalies and defects that result in complex load redistributions within the finished structure. Being

able to relate composite failures to these local strain redistributions, local damage states, and global loading is a necessary step in improving our understanding of the health of the structures. A better understanding on the health of a structure would require: (1) development of sensing systems (mounted or embedded) capable of identifying and quantifying damage that may lead to changes on the performance of the structure in question; (2) development of techniques that can verify the validity of the signals produced by the sensors under different operational conditions; (3) mathematical algorithm and systems capable of dealing with large amounts of data in order to quantify trends in the measured parameters; and (4) and most likely the most challenging step, is the development of a holistic physics based understanding of damage growth due to fatigue under different operational conditions.

Structural Health Monitoring (SHM) is defined as “the process of acquiring and analyzing data from on-board sensors to evaluate the health of a structure” [2, page 4]. A change in the load carrying capacity of the structure can be an indication of a change in the health of the structure. The aerospace community is considering the use of SHM in order to implement a Condition Based Maintenance (CBM) approach on critical components. The final objective of SHM, is the identification and quantification of damage. Unfortunately, many SHM technologies have not achieved widespread acceptance due to unresolved conditions such as for example: (1) lack of reliability of the sensors and uncertainty of the obtained measurement [3–5]; (2) requirements established by the certification authorities on the implementation of SHM systems [2]; (3) lack of Probability of Detection (POD) curves for specific sensor network at specific locations of the aircraft, in addition to the associated costs required to generate these POD curves [6]; and (4) lack of understanding on the significant effects that environmental operational conditions (EOCs) and geometric complexity of the structure have on the ability of many SHM systems to properly and accurately detect and localize damage [7, 8, 9].

In the case of Unmanned Aerial Vehicles (UAVs), structural health and load monitoring is envisioned due to the larger use of composite materials on these structures [10, 11]. UAVs lack in many cases the historical background of loads and flight envelopes compared with traditional commercial aircrafts or fighters [11, 12]. In the aerospace industry, load monitoring of critical components are evaluated through the use of Operational Load Monitoring (OLM) techniques, utilizing Flight Parameters-Based methods and traditional Strain Gauges (SGs) sensors [13]. These methods make use of the flight state data acquired from on board accelerometers and gyroscopes. The accelerometer and gyroscope data in combination with transfer functions are used to relate the flight maneuver to strain data on critical aerospace structures. These OLM can provide only a global load state, while SGs are able to provide localized strain data; however monitoring of more than few locations can result in weight penalties.

Many researchers have considered the embedding of fiber optic sensors in composite structures, and their effect on the structural performance. By testing equivalent specimens with and without the fiber optic sensors, various studies concluded that there was no negative effect in the mechanical structural properties (strength, strain-energy release rate, etc.) [14, 15]. However, other authors presented evidence of localized effects such as material relaxation and higher stress concentration around the sensor [16, 17]. The effect on the presence of the fiber embedded in a composite structure is dependent on several factors such as: lay-up sequence, thickness, material matrix and fiber type. In addition to the effect on the structural performance, there are a series of associated manufacturing issues with the embedding process. The embedding of fiber optic sensors in composite structure has been primarily performed as a manual operation during the laying up of the composite fabric, increasing costs of instrumenting the structure [18]. A positive outcome of this manual embedding procedure is the greater cohesion achieved between the composite material and the fiber optic sensor [19, 20].

Many researchers have concentrated their efforts on the use of Fiber Bragg Grating technology [21, 22], also known as discrete sensing system. However, a second generation of optical sensing system, known as Distributed Sensing Systems (DSS) is being considered for strain/temperature monitoring applications [23, 24]. DSS have the primary advantage of being able to obtain strain/temperature measurements along a commercial fiber optic sensor with no gratings. The DSS technique is based on the principle of Rayleigh, Raman or Bragg backscattering, which are produced by different type of interactions of the light photons traveling inside the fiber core and thus generating backscattering of different wavelength [25]. DSS make use of the light reflections generated by inherent characteristics of the fiber material (interference data), which are then used to compute changes in strain and temperature [25]. Each fiber has a specific local geometry or impurities distribution, in a non-strained state, thus providing a reference backscattering profile. When an external strain and/or temperature field acts on the fiber, the local refractive index of the fiber is affected. Thus, the strain or temperature field causes a different backscattering profile. Comparing both the baseline and strained profiles, it is possible to translate the differences into changes in strain and temperature measurements.

The DSS Rayleigh backscattering system used in this study consists of an Optical Frequency Domain Reflectometer (OFDR), which is used to analyze the local backscatter light intensity (interference data). The OFDR consists of a tunable laser source, a Fast Fourier Transform (FFT) analyzer, a scope and a photo receiver. The OFDR is connected to an optical fiber optic line with no gratings. The fiber optic line is connected to the structure being evaluated. The interference data is collected in the frequency domain and analyzed via the FFT analyzer. However, a subset of the interference data is used to determine a cross correlation between the measurement and the baseline frequency spectrum. This comparison between the measurement and the baseline frequency spectrum is used to determine if there has been a frequency shift in the Rayleigh scatter pattern, which is proportional to a strain change.

Due to the complex and anisotropic behavior of composite structures, high strain and stress gradients can appear even at low loads. Despite some of these advantages, current DSS fiber optic data acquisition systems are heavy and bulky, thus presenting a major limitation in day-to-day use and operations in load monitoring of UAVs. Furthermore, the signal processing can be challenging due to the overwhelming amount of data that can be collected and processed. With Rayleigh backscattering DSS, it is possible to monitor a strain or temperature point every 1.25 mm in a 10 meter fiber at a maximum acquisition rate of 23.8 Hz, or every 5mm up to 10 meters in length at 100 Hz [26].

Due to the lack of UAV load spectrums available in the literature, the use of DSS technique would allow for better understanding of the typical load spectrums required to withstand by UAV structures and thus provide the aviation authorities the necessary information about UAVs for future commercial use [27].

Many challenges still present themselves in applying the technology to real structures. This paper examines these challenges in the context of a UAV wing structure. The capabilities of a Rayleigh backscattering fiber sensing system for determining strain and resolving loading are investigated in this manuscript. This study focuses on the application of this technology on a real structure, including challenges in embedding the sensor during manufacturing, qualifying/verifying the performance of the sensor after manufacturing, and the performance of the embedding sensor under dynamic loading which are representative of typical flight loading scenarios. In addition, apart from the instrumented wing prototype, a second non-instrumented wing was manufactured in order to study the effect of the optic fiber on the structural performance. The aim of this work is to identify and highlight specific challenges for the successful application of the technology for real-time load monitoring of UAV structures. The primary scientific objective of this study was to investigate the capabilities of Rayleigh backscattering for strain measurements in static, quasi-static and dynamic

loading conditions utilizing an optical sensor embedded in a composite UAV wing. Finally, a FEM was developed with the aim to simulate and predict the wing structural performance and assist the research team in verifying the experimentally obtained results.

Wing Design Concept

The front wing of a tandem UAV named Dragonfly was the structure selected for the integration of an Optical Fiber (OF) sensor in order to determine the capabilities of a Rayleigh backscattering Load Monitoring System. The UAV, whose preliminary design was developed at the Faculty of Aerospace Engineering at Delft University of Technology (TU Delft) [28], has a sailplane configuration with the ailerons located in the front wing as shown in Fig. 1.



Figure 1. Illustration of the Dragonfly Unmanned Aerial Vehicle [28]

The relevant geometric features of the wing and aircraft for this work are shown in Table 1. A sketch of the top view of the wing from the UAV symmetry plane is shown in Fig. 2, illustrating the size and location of the aileron and servomechanism cut outs.

Table 1: Main Dragonfly Geometric Features

UAV estimated mass	10.9 kg	Aileron Airfoil	Eppler 582
Front Wing Airfoil	Eppler 582	Aileron span, b_a	0.475 m
Front Wing Span, b	2.55 m	Inner aileron position, b_{ai}	0.77 m
Front Wing Chord, c	0.1475 m	Aileron Chord	0.061 m

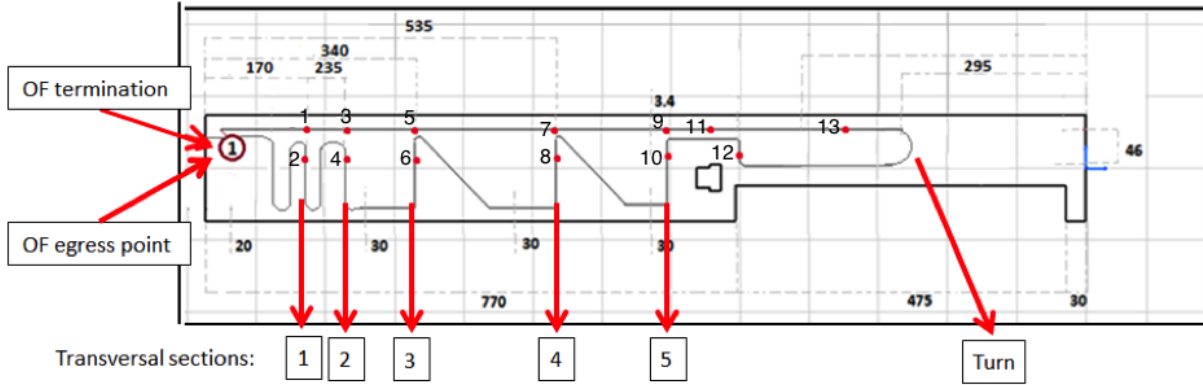


Figure 2. Optic fiber lay-out with the corresponding Strain Gauge (SG) numeration and location at specific wing stations (measurements in mm). Overall wing length is approximately 1300 mm by a chord length of approximately 150 mm

The wing structure consists of a high stiffness foam core and a composite outer skin laminate made of Unidirectional Carbon Fibers (UDCF) and E-glass weave (EGW) layers. Taking the wing length as the reference direction, the skin laminate was (from suction to pressure surface): $\pm 45^\circ$ EGW, 0° UDCF, Core, 0° UDCF, $\pm 45^\circ$ EGW. In order to define the material behavior in the FEM model, a thorough structural characterization of both foam and composite shell, were carried out at Delft Aerospace Materials and Structures Laboratory (DASML). A detailed description of the test procedure and standards employed can be found in [29]. The properties obtained and the commercial constituent material names are listed in Table 2 and 3.

Table 2: Mechanical properties foam core (T-Tension, C-Compression).

Foam: Airex R82®					
E	ν	S^T	ϵ^T	S^C	G
99.7 MPa	0.4	2.6 MPa	$3.1 \cdot 10^4 \mu\epsilon$	-1.4 MPa	31.4 MPa

Table 3: Mechanical properties of the composite skin (T-Tension, C-Compression).

Composite Skin: UDCF UDO CST 300/300 The Carbon Group EGW HexForce 7581 Hexcel					
E_1	ν_{12}	S_1^T	ϵ_1^T	E_2	S_2^T
72.9 GPa	0.3	1190 MPa	$1.4 \cdot 10^4 \mu\epsilon$	10.8 GPa	132 MPa
ϵ_2^T	S_1^C	ϵ_1^C	S_2^C	ϵ_2^C	G_{12}
$1.9 \cdot 10^4 \mu\epsilon$	403 MPa	$0.98 \cdot 10^4 \mu\epsilon$	178.3 MPa	$2.1 \cdot 10^4 \mu\epsilon$	4.3 GPa

Wing Fabrication and Optical Fiber Sensor Embedding

The UAV wing was manufactured to scale. The airfoil shape of the foam core was manufactured using a CNC milling machine. After machining, the core did not require a sealing step due to its closed-cell nature. The dry carbon composite layers were draped over the core prior to adding the glass fiber fabric. Next, the OF was routed over the wing surface and locally secured in place using the same epoxy resin that would later be used to infuse the overall wing. The OF integration process was defined and implemented based on the following literature sources [28,30,31]. Both the ingress

and egress portions of the OF were protected with a Teflon tube in order to protect the sensing fiber at these critical locations. The glass fabric layer was subsequently draped over the wing, embedding the fiber between the carbon and glass layers. The wing was covered with a vacuum bag which was sealed, protecting the OF connector and egress point. An auxiliary vacuum bag was created around the connector in order to create vacuum around it, thus avoiding any air coming into the wing through the connector during the infusion process. The infusion process was followed by a 24 hours curing at room temperature (20°C) followed by a 6 hours curing at 80°C. Finally, the vacuum bag was removed and the leading and trailing edge were sanded to remove any excess epoxy resin.

The routing of the OF in the wing is defined in Fig. 2. The bending loads, which appear in a wing under lift, are carried out through normal stresses along the wingspan and were monitored through the longitudinally placed fiber segments. The transversal direction, although less loaded than the longitudinal one, carry the torsional loads and were also considered with this fiber layout. Transversal segments were placed at different wing cross sections (sections 1 through 5 as shown in Fig. 2). Finally, in order to assess the presence of torsion due to alignment issues with load introduction, 45° oblique segments were also laid at different sections of the UAV wing. Both the OF connector and termination end are indicated in Fig. 2 as point 1. The connector ends of the OF sensor attaches to the Optical Frequency Domain Reflectometer through an LC/APC connector as shown in Figure 3.

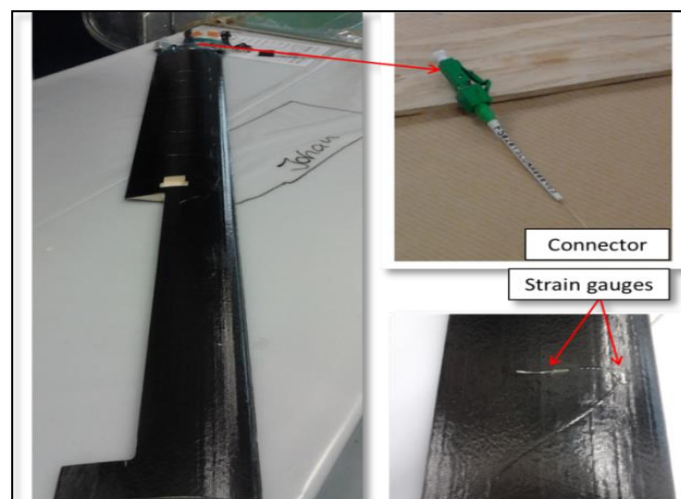


Figure 3. Dragonfly UAV Wing with the LC/APC connector and surface mounted strain gauges

A secondary and equivalent non-instrumented wing prototype without the OF sensor was also manufactured. The manufacturing process followed the same procedure (resin infusion and curing parameters).

Experimental Set Up and Test Cases

In order to verify the capabilities of the OF integrated sensor and assist in the verification of the FEM, the test wing containing the OF was instrumented with 13 Strain Gauges bonded at the suction surface over the OF route as shown in Fig. 2. The tests were performed using a 10kN fatigue frame. A Luna Optical Frequency Domain Reflectometer with Software Version 2.02 was used for this research study. The complete set up can be seen in Figure 4. An aluminum frame was built in order to support the wing and connect it with the testing frame (Figure 4a and b). A high

stiffness polymer fixture was manufactured and attached to the supporting frame. The testing bench was connected to the prototype by means of an auxiliary load cell (Figure 4c).

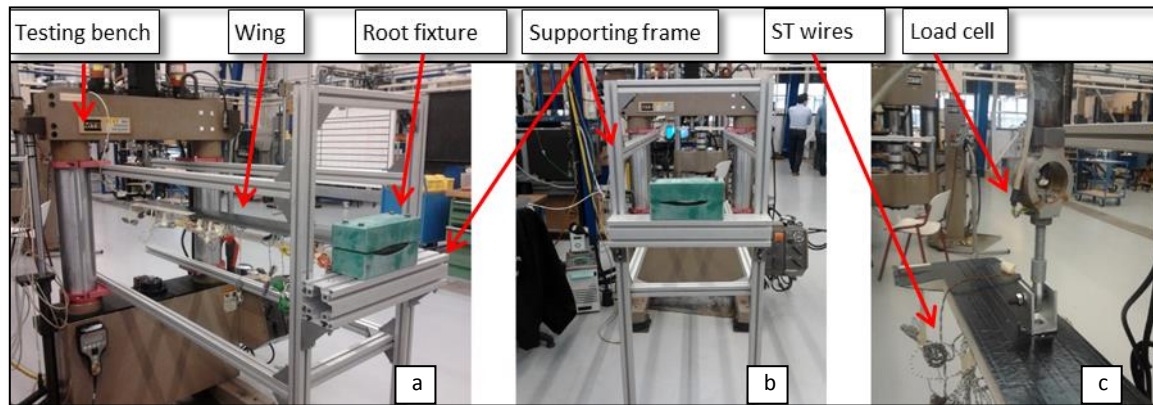


Figure 4. a) Testing and supporting frames with the one prototype clamped; b) Front view of the supporting frame and clamping fixture; c) Detail of the auxiliary load cell

Three test cases were considered as part of this study:

1. Simple Static Bending Loading Conditions: The wing was tested simulating the cruise and maneuver condition applying upward displacements. The relation between loads and displacements were obtained from a FE model developed in ABAQUS™. At the load cell location (200 mm from the wing tip), 30 and 50 mm of displacement in the vertical direction were applied in order to simulate bending loads due to cruise and maneuver flight conditions in subsequent static steps of 5 mm.

2. Low Frequency Bending Loading Conditions: With the aim of studying the OF capabilities under dynamic conditions, a series of bending tests were performed at different frequencies (0.02, 0.05, 0.1, 0.2, 0.5 and 1 Hz) applying a 30 mm displacement at the cruise condition.

3. Effect of Embedding of Fiber on Composite Structural performance: In order to understand the long-term effect of embedding of a fiber optic on the structural performance of the wing, a series of static tests were considered. In addition, a fatigue test simulating 6 years of UAV operation [28] was carried out by subjecting the structure to 18,000 loading-unloading cycles of 40 mm of displacement (1.33 times the normal cruise load).

The simple static and low frequency bending tests were also performed with a non-instrumented prototype wing and the results of both specimens were compared by means of the strain gauge measurements.

Finite Element Analysis Verification Model

In addition to the experimental test conducted, a Finite Element Model was developed in order to better understand the structural behavior of the composite UAV wing and thus verify the strain distribution obtained from the OF sensing system.

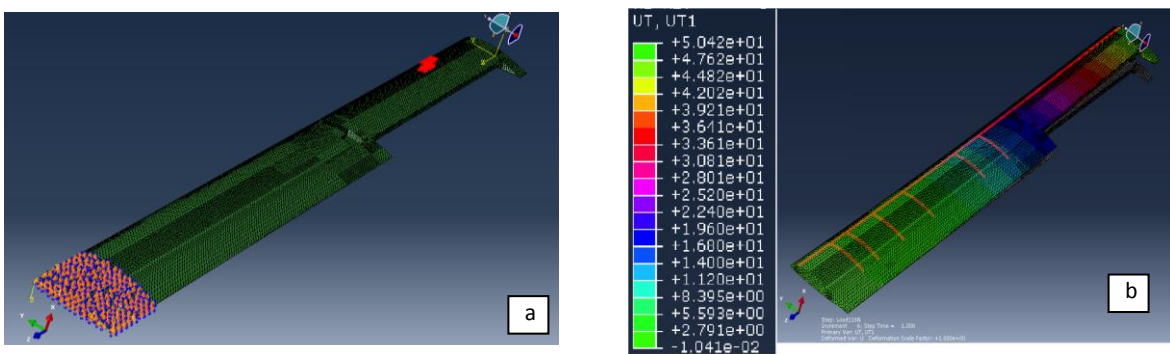
The wing was modeled in ABAQUS™ 6.13. The structure was initially designed in two 3D deformable parts consisting of a solid core and a planar shell. These parts were meshed employing quadratic tetrahedral elements, C3D10, and quadratic triangular thin shell elements, STRI65 respectively. Quadratic elements were chosen due to their ability to better capture the bending nature of the test. The STRI65 element was selected based on its performance for thin curved shells in bending problems. Element geometrical distortion, such as excessive aspect ratio can be a source for the lack of accuracy. The mesh was refined primarily in two main areas of interest. The first

region was focused around the root of the wing, while the second region consisted of the servo and aileron cutout section. Finally, a mesh convergence study was performed on the FE model in order to guarantee good convergence of the computed strain values.

The material properties from Table 2 and 3, contain the data used for the foam (defined as linear isotropic material) and composite skin (anisotropic lamina). These properties were assigned to the 3D and 2D element mesh. In the case of the skin, also the composite lay-up and orientation were defined for both the suction and pressure surfaces of the wing.

The boundary conditions for this model consisted on clamping the wing root (by means of the support fixture) while applying a load close to the tip of the wing as shown in

Figure 5a. The steps in ABAQUS™ were defined as linear steps. However, at the highest loads, geometric nonlinearity was considered. The wing initial state can be seen in Fig. 5a while the deformed states under the maximum applied cruise load of 116 N resulted in a vertical displacement (U_{T1}) of approximately 50 mm as shown in Fig. 5b. This displacement distribution shows only a couple of millimeter deflection in bending close to the root of the wing. However, the deflection increases considerably in the cutout section of the wing (the aileron region).



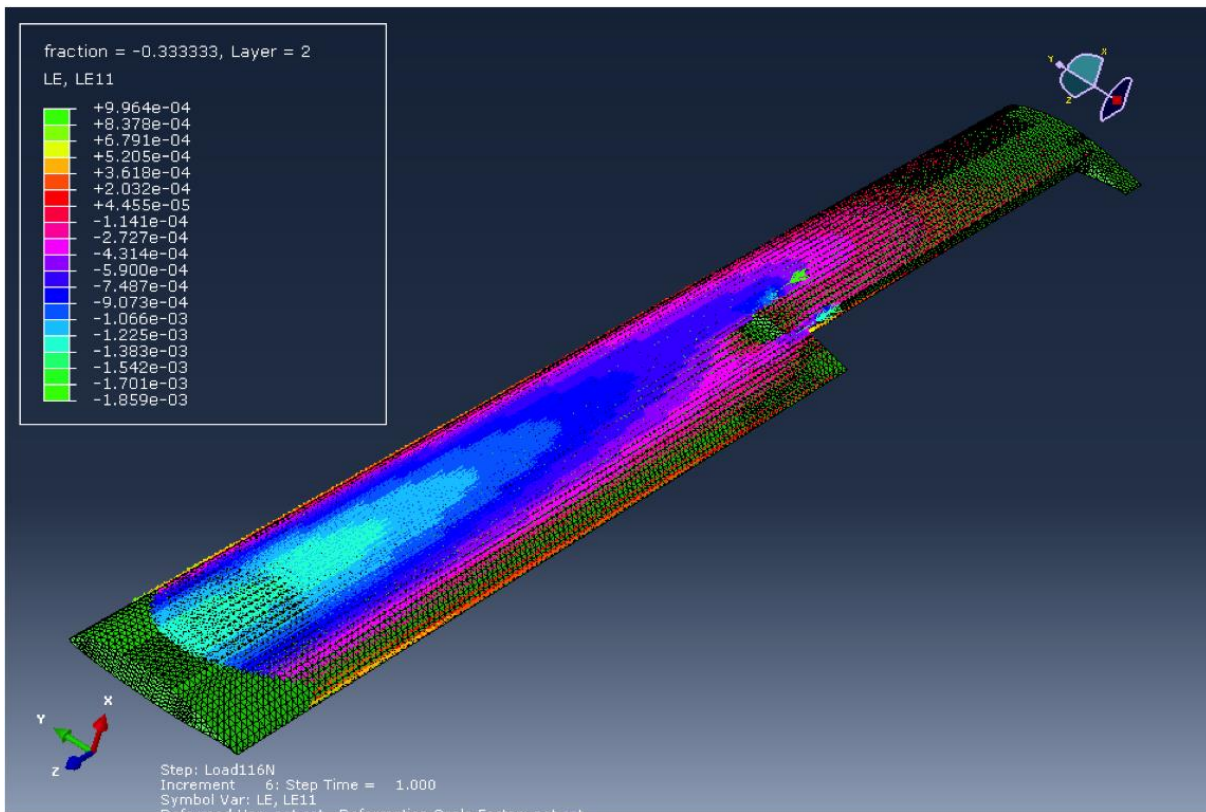


Figure 6. Deformed state under 116 N. Longitudinal strains symbols, Le11

Experimental Results

1. Simple Static Bending Loading Condition: The measurements obtained from OF under simple static bending loading conditions were evaluated using Matlab™ in order to obtain clean strain profiles. The profiles obtained from the static bending tests are presented in Figure 7. The strain is measured in micro-strains along the whole sensor length at different applied load-displacements (every 5 mm up to 30 mm tip displacement). The initial and final fiber segments (around 0.3 and 3 m respectively) show very low deformation levels due to the clamping fixture. From the OF egress point, a large negative strain peak (as high as 650 micro-strain at 30 mm tip deflection) corresponds to the fiber segment under compression, that is the suction surface under lift loads as documented in [32]. The positive strains belongs to the transversally placed OF segments, and their value measure the material Poisson's effect of the wing. As shown in Figure 2, from approximately 2 meters to the termination end, the system measures the bending strain along the wingspan. Despite the noise obtained in certain sections of the span of the fiber, a clear strain profile is visualized. The accuracy of the measurement was then compared to strain gauges placed on the surface of the wing as follows.

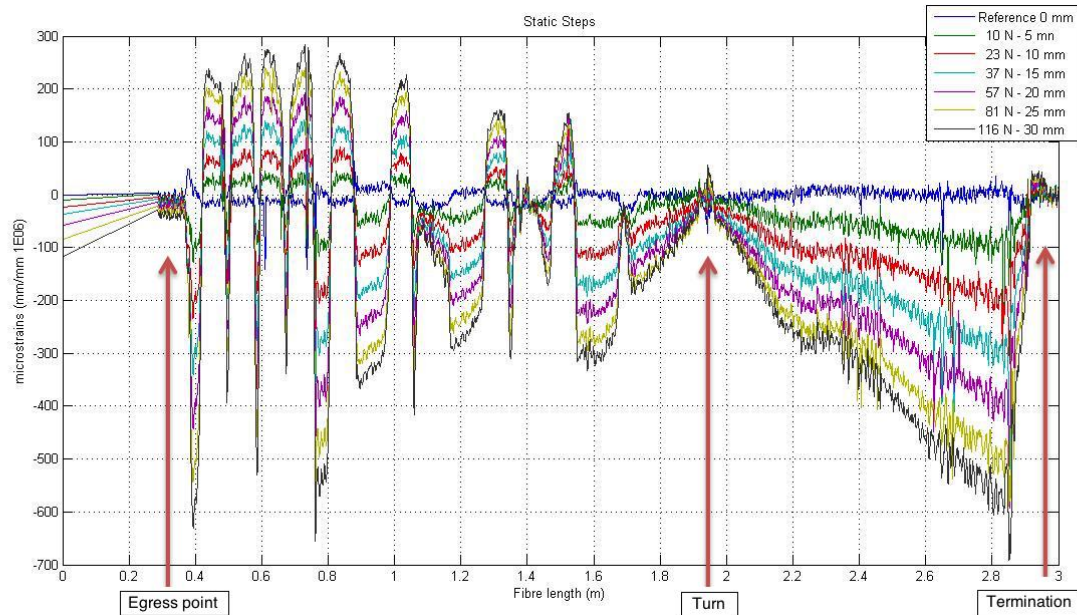


Figure 7. Optic fiber strains along the whole sensor length under different static loads. The legend addresses the loads-displacement equivalence

As part of the initial analysis a 10 N bending load applied at the tip of the wing was used to compare the strain values between the FEM results and those obtained experimentally from the OF and SG system. The strain obtained from the FEM, is measured at the surface of the wing where the strain gauges were placed (SG FEA model). However, the strain measurement of the embedded OF in the FEA model was taken at the interface of the carbon and glass fiber (OF FEA model). Continuous smooth lines shown in Fig. 8, depict the strain measurements obtained from the FEA. The OF experimental strain results are shown in the same figure as a 20 micro-strain band that follows the same trend as the FEA results. It is important to note that the strain at the root of the wing contains the termination of the fiber. Thus, the highest strain is sensed at approximately 2,850 mm length of the fiber optic sensor. The SG results are depicted in the same figure as a series of diamond dots. The figure depicts good agreement between the numerical and experimental techniques. However, the OF measurement is filled with noise throughout the entire strain profile. In addition, it is interesting to note that the OF measurement falls between the FEA results and those measured by the strain gauges. The most significant difference (error) occurs at the root of the wing between the FE model and the strain gauge (approximately 100 micro-strains), while the OF measurement falls in between these two results. However, it is important to note that this error occurs at the lowest applied load (10N) thus resulting in a small change of strain on the structure. Other sources of error between the FE model, the strain gauge results and those of the OF system, may be attributed to inaccuracies in selecting the same position on the structure for comparison with the other obtained values (SG and FEA model). This is more significant in regions of high strain gradients such as the root of the wing. The OF system, has a position measurement resolution along the length of the fiber of ± 1.3 mm. In addition, when the fiber optic is embedded or bonded on the structure, there is a need to identify the position of the fiber optic line with respect to its location on the structure. This is usually performed by pressing on the fiber with the operator's finger to identify a peak value of strain and thus identify that position of interest along the fiber length during testing. If the fiber is embedded this position might not be as easily identified. Finally, it is important to note that the section of the root of the fiber optic sensor is close to a compressed region as shown in Fig. 4a (root fixture), which could alter the strain measurement around that section.

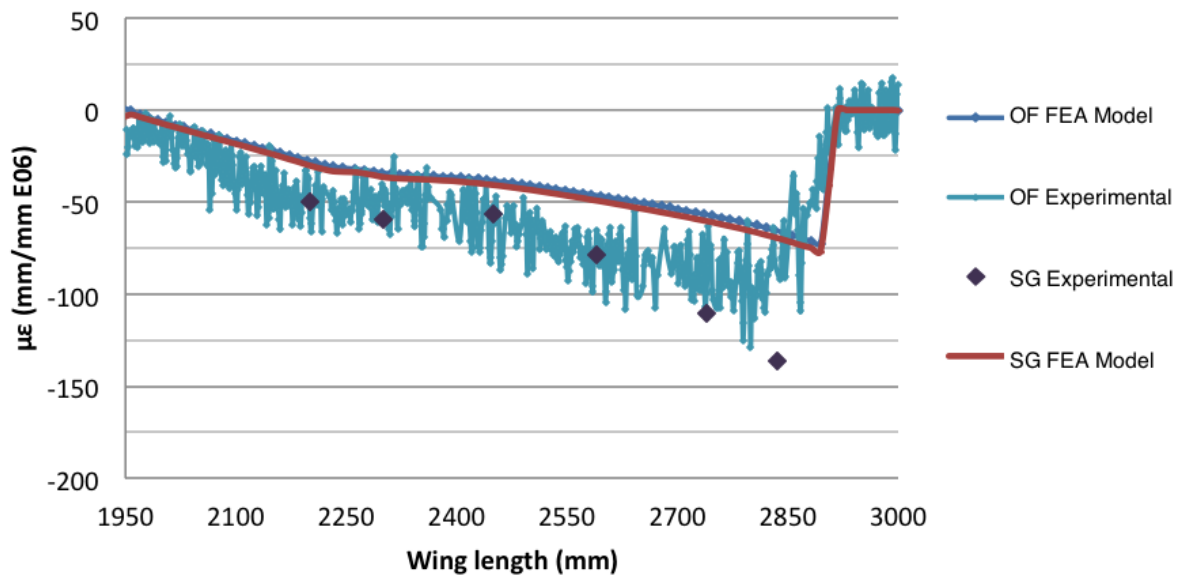


Figure 8. Strain (ϵ_{11}) along the wing length, model-experimental results comparison at 10N

Fig. 9, shows the longitudinal profile strain at 81N. As shown in this figure, the higher the load, the noise band of the optical fiber is not as noticeable, primarily due to the higher overall strain level that the structure has been subjected to. However, both the FEM and the experimental results match the strain distribution profile. At the higher values of strain (closer to the root) the peak values of strain are underestimated by approximately 20% difference when compared to values obtained from the SG. It is possible to observe that the strain profile of the OF follows that of the FEA model. The OF system, again misses the high peaks captured by the strain gauge and the FE model. In this figure the difference in measurement between the OF system and the strain gauge is of approximately 150 micro-strain.

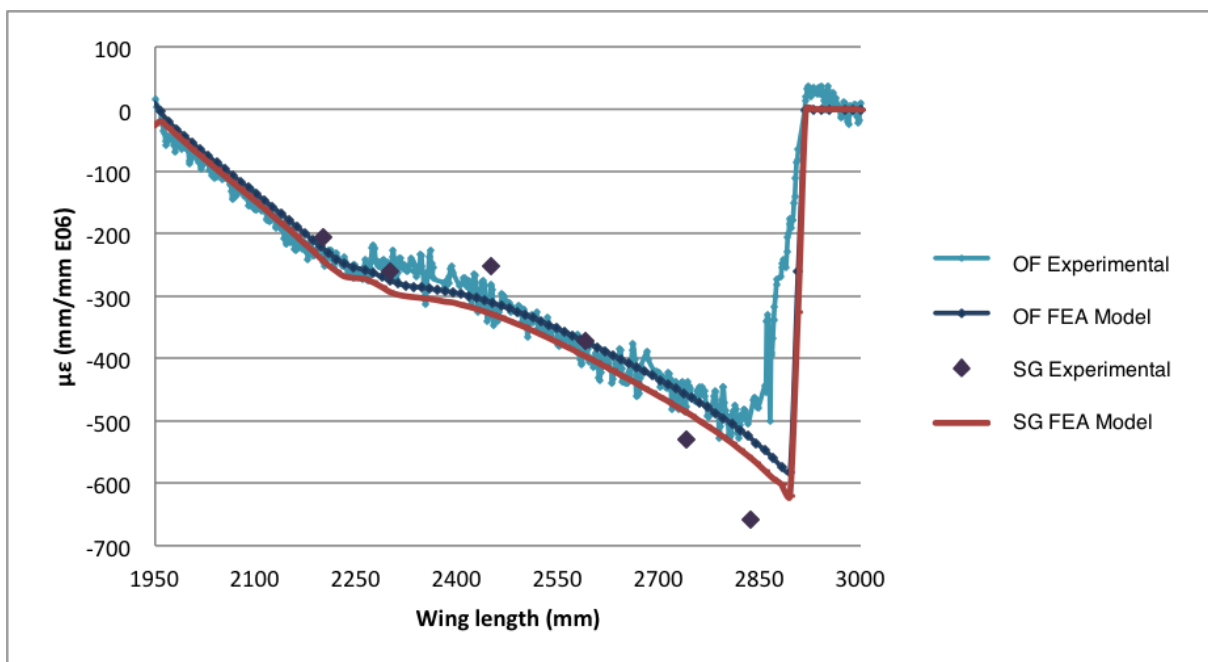


Figure 9. Strain (ϵ_{11}) along wing length, model-experimental results comparison at 81N

Fig. 10 shows a close up comparison of the strain measured with the Optical Fiber (OF) and that of the strain measured with commercial off the shelf strain gauges (SG) for different load levels. The strain profiles were measured at 116 N, 81 N, 37 N and 10 N. As expected and shown from the

FEM the trend was more pronounced closer to the root of the wing where the strain values are higher. Analyzing the wing tip region, it is possible to see that both the OF and the SG tend towards zero strain, as it is expected for this type of structure. On average, the OF measurements underestimate the SG measurements by approximately 14% difference. The exception to this underestimation occurs on SG 5 and 7 whose measurements were slightly smaller than the OF.

Fig. 10, does not include any of the FEM values. As part of our analysis we deformed the wing to an applied load of 116N in order to determine at which load level the FEM results and the experimental values would diverge. At higher values of applied bending loads (greater than 81N) the FE model does not capture the material non-linearity. However, the results indicate that the strain profiles at different load levels and those of the SG are in good agreement, with the exception of the peak strain values at the root of the wing. It is expected that this difference in values at the roots be primarily due to the compression of the fiber optic by the clamping fixture.

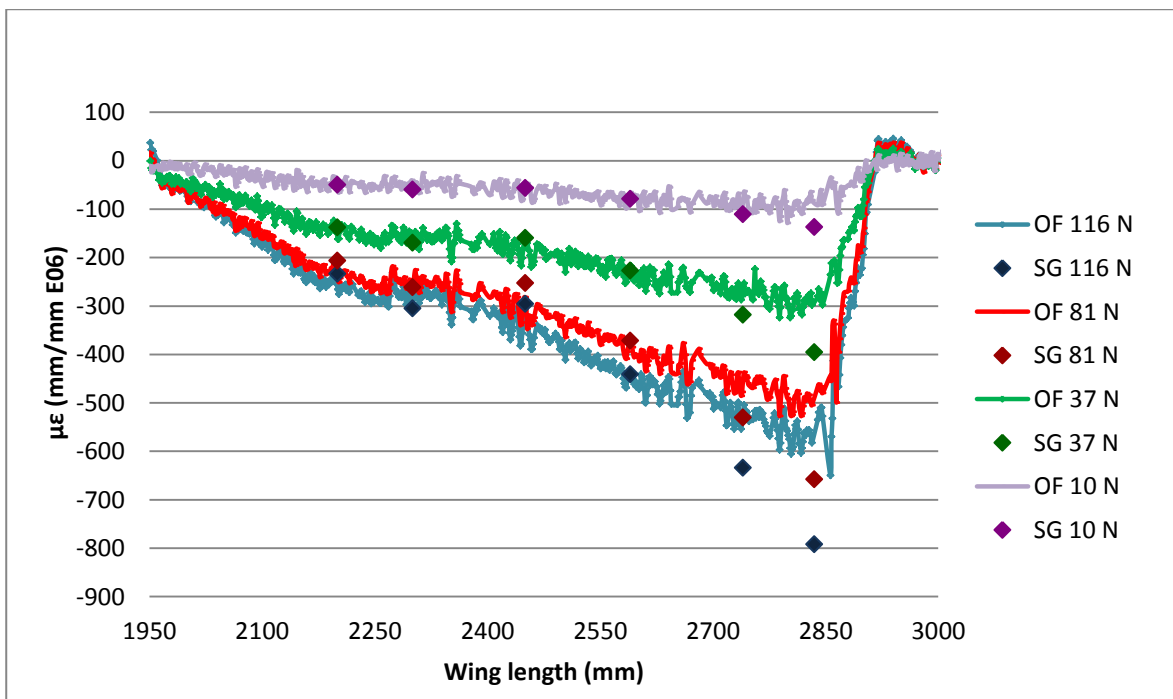


Figure 10. Optic fiber and SG longitudinal strains (ϵ_{11}) at different static loads

In addition to the longitudinal strain, the transversal strain profiles were also analyzed and compared to the SG results. Figures 11 and 12, shows the OF segment transversal strain profile and its equivalent strain gauges value at different loads for Station 1 and 5 respectively. Only the areas of the wing length and wing chord where the OF was embedded are shown. In this same figures the FEM results are depicted. The results of the model follow the same trends as those observed from the experimental results obtained from the OF system. The average dispersion of the model with respect the OF and SG measurements is 14.7%, which was linked to differences between the real clamping fixture (unnoticed clearance or slight clamping pressure variation between tests) and the idealized boundary condition. It is important to note that the model allows for capturing strain in locations where the OF sensors was not placed between 0 and 25 mm and 90 and 140 mm. The strain measurement obtained from model were taken at two location: (1) at the Strain Gauge Ply, outer most fiber and; (2) at the inner ply where the OF was placed. The model results are at the two different plies (OF FEA model and SG FEA model).

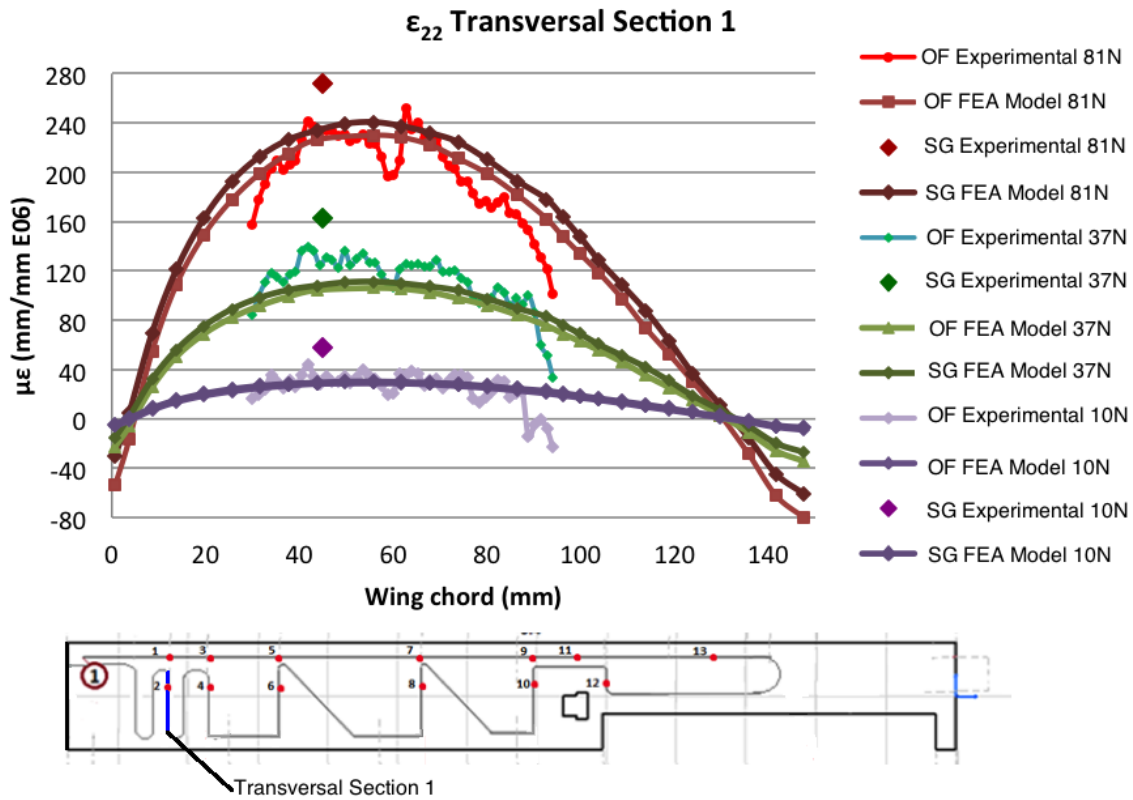


Figure 11. Optic fiber and SG transversal strains at different static loads (Station 1)

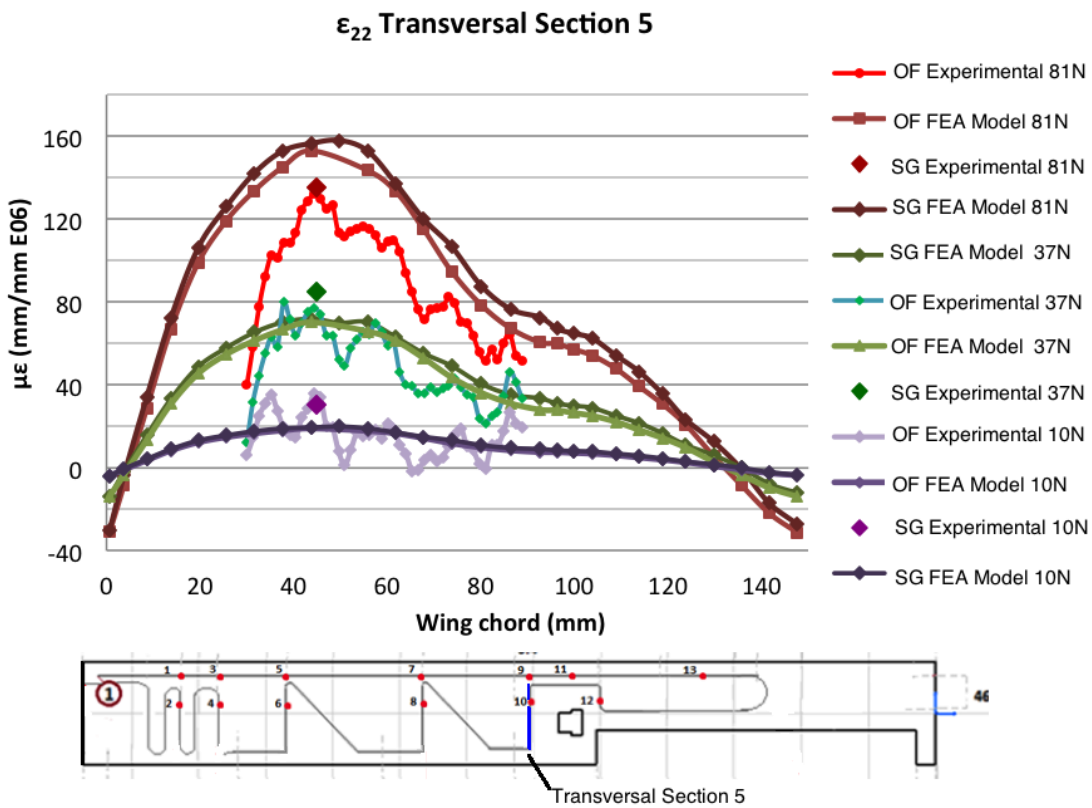


Figure 12. Optic fiber and SG transversal strains at different static loads (Station 5)

Taking into account the strain differences produced between the OF sensing system, the SG and the model it is obvious that the embedded OF sensor is able to capture accurate strain profiles of a

representative aerospace structure. Furthermore, a significant advantage of the OF system is its ability to capture a distributed set of strain measurements along the length of the fiber (over 2000 points vs. 13 SG).

Table 4: Average Percentage Difference. Values were obtained by comparing at each location and load step the OF-ST measurements for the experimental column and the model strains at the OF and SG locations in the laminate.

Strain	Percentage Difference between OF-SG experimental results	Percentage Difference between the OF-SG location in the FEM %
ϵ_{11}	10.3	6.9
ϵ_{22}	13.7	7.3

Low Frequency Bending Loading Condition

The results of the dynamic performance of the Rayleigh backscattering are presented in the figures below. This dynamic evaluation was considered after observing high noise peaks in the strain profiles during dynamic testing (e.g. low amplitude but relatively fast movement). These noise peaks did not correspond to real strain values experienced by the wing. The following graphs showed the data collected by the OF at four of the dynamic tests without applying any noise filter. The data was acquired continuously at the load levels corresponding to the previous static test. The data shown in the graphs were extracted during the low frequency bending loading conditions. Figure 13, show the strain distribution at a loading frequency of 0.02 Hz. The results shown in this figure clearly shows a clean strain profile.

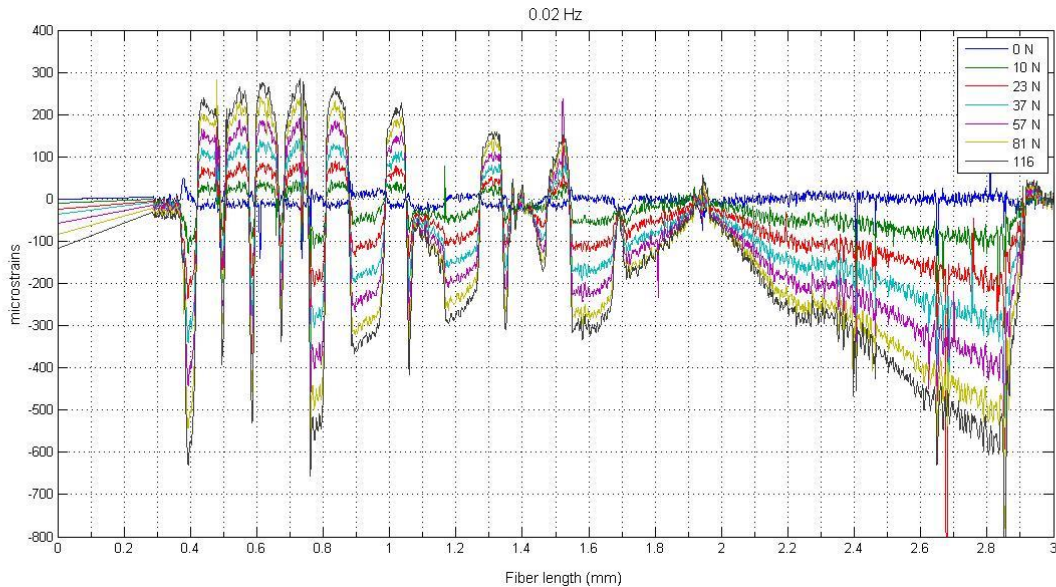


Figure 13: Load steps at 0.02 Hz. The strain range at 0.2 Hz is between 400 and -800 $\mu\epsilon$.

A second test was performed at an actuation frequency of 0.1 Hz. The results of these tests were still readable and a clear strain distribution for the different sections of the embedded fiber was obtained at all applied loads.

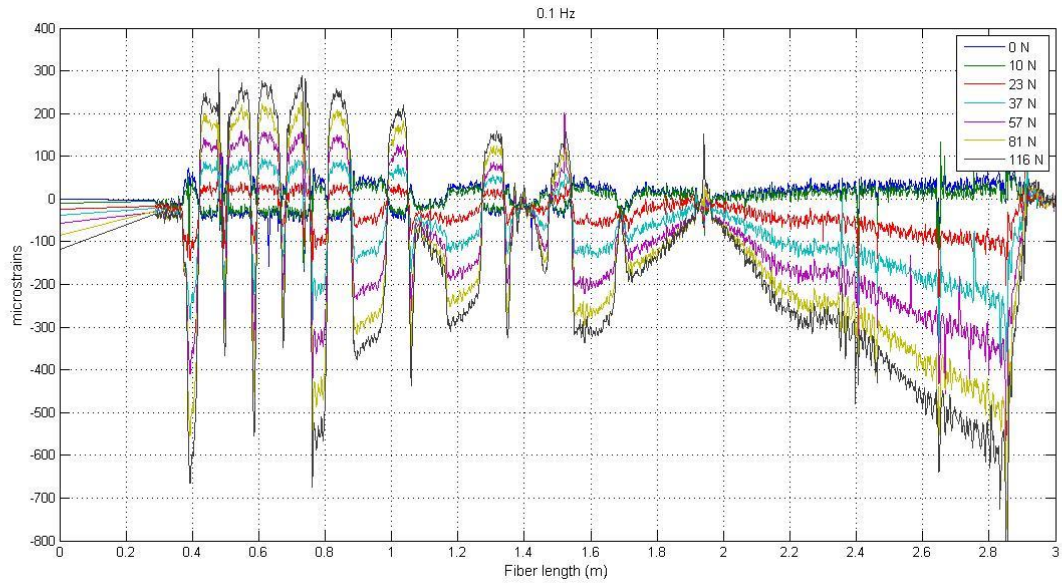


Figure 14: Load steps at 0.1 Hz. The strain range is between +400 and -800 $\mu\epsilon$.

However, at a dynamic loading frequency of 0.5 Hz (Fig. 15) the profile becomes very noisy and the challenge to interpret the strain distribution becomes very noticeable.

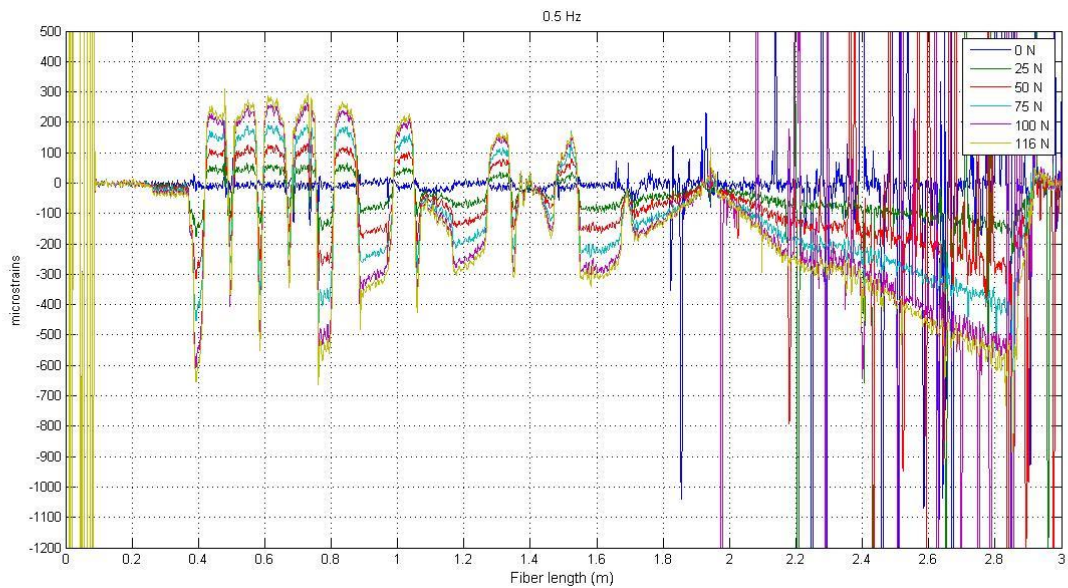


Figure 15: Load steps at 0.5 Hz. The strain range at 0.5 Hz is between +500 and -1200 $\mu\epsilon$.

Finally, in Fig. 16, most of the data obtained using the OF system is filled with noise, thus creating a significant limitation for the use of this system for dynamic testing even in what would be considered low frequency dynamic test conditions for structural applications of aerospace structures.

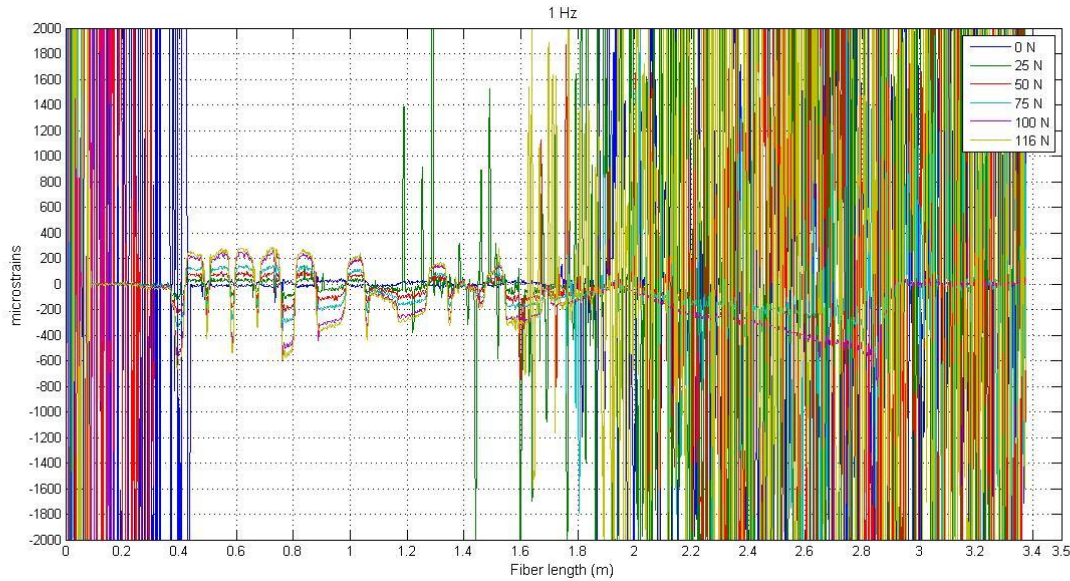


Figure 16: Load steps at 1 Hz. The strain range at 1 Hz is between +2000 and -2000 $\mu\epsilon$.

As seen in Figures 15 and 16, the higher the dynamic actuation frequency of the structure the worse the strain measurements obtained. As previously discussed, during Rayleigh backscattering strain measurement, a subset of the interference data is used to determine a cross correlation between the measurement along the fiber optic line and the baseline frequency spectrum previously recorded. This comparison between the measurement spectrum and the baseline frequency spectrum is used to determine if there has been a frequency shift in the Rayleigh scatter pattern, which is proportional to a strain change for that section of the fiber. This frequency shift between the baseline spectrum and the current measured spectrum is calculated through a search algorithm, which looks at frequency phase shifts of cross-correlation peaks between the two spectrums. However, as the structure being evaluated is under motion or vibrational loads, the fiber optic sensor is also exposed to these same motions and vibrations, thus creating a change in the optical length during the data acquisition scan. When the optical phase at the measurement point of the fiber is offset by approximately $\pm\pi$, the correlation peak strength is diminished leading to excessive noise levels in the measurement.

Effect of Embedding of Fiber on Composite Structural performance

The effect of embedding the sensor on the structural behavior was also analyzed. The strain measurements of the instrumented and non-instrumented wings were compared at every load steps. The results of this comparison showed that the instrumented wing showed considerably higher strains under the same loads almost at every point of the locations analyzed. It was especially noticeable in the longitudinal direction, where up to 32% of difference appeared at the wing mid-section. On average, the OF instrumented prototype was found to be 23% less stiff than the non-instrumented wing. However, although there were differences in the strains values, both specimens showed very similar behavior regarding hysteresis during the load-unload cycles of the static tests, as well as repeatability in their responses. In both prototypes, less than a 4.4% of difference was found between load-strains curves at different load-unload cycles.

In order to understand if the fatigue tests had any detrimental effects on the OF performance a set of subsequent static tests were carried out. The loading-unloading cycles were applied at 1 Hz frequency and every 1000 cycles the OF strains profiles were acquired at static maximum and minimum displacements. The results produced almost overlapped strain distribution profiles. Furthermore, the load necessary to achieve the desired displacement didn't change during the fatigue test in any of the prototypes and therefore no decrease of the structural performance was

experienced by the OF sensor. In the final static tests the SG and OF measurements of the instrumented prototype as well as the SG of both wings were compared between each other's obtaining very similar results to those in the first set of tests (same SG-OF offsets and higher strains in the OF wing under the same loads).

Discussion

An Optic fiber distributed sensing system was integrated through embedding in the skin of a composite UAV wing. The manufacturing-integration process developed for this particular application technique ensured the OF integrity and allowed its posterior usage.

After signal processing, clear measurements could be obtained from the embedded sensor while the prototype was subjected to static loading conditions. The wing was also instrumented with strain gauges, considered the "golden" industry standard. Both measuring systems showed the same trends in strain profile at every load level. The OF measurements were verified at every location where the SG were located. The OF generally gave smaller results than the SG. However, with the help of the FEM, the actual strain difference between the OF and the SG was shown to be due to where the measurement was taken, at the upper extreme surface or in between the carbon/glass fiber ply along the wing cross section (see Table 4).

The FE model outputs were compared with the experimental results. The model made use of the strain at the OF ply and at the surface of the wing. The experimental results showed to differ from the FEM on average by approximately 14.7%. This finding was considered a good level of approximation due to the complex core-composite skin interaction. The load monitoring capacity has been significantly increased compared to the data obtained from previous discrete sensors without increasing the structural weight. In addition, the wiring complexity was significantly reduced in comparison to the utilization of regular strain gauges. Furthermore, the embedded fiber is a standard commercial fiber with no gratings.

The load monitoring capacity of a distributed sensing system has an enormous potential in terms of providing strain distribution profiles for complex structures. In our test case, our UAV wing did not approach any critical loads (the maximum compressive strain obtained was lower than $800 \mu\epsilon$ being the compressive failure at $9800 \mu\epsilon$). The data obtained from the OF sensor together and the existence of a FEM, allows for a complete understanding of the structural integrity of the wing.

It was observed that the embedded sensor had a negative effect on the structural stiffness. However, the laminate used in this work consisted of only two composite layers, and therefore in thicker laminates the interference would be surely reduced. In addition, the sensor presence didn't affect the response repeatability for long term usage, which was another positive outcome observed as part of this study and the potential implementation of this technology in the field.

During the dynamic tests results, it was observed that the quality of the data acquired decreased considerably after 0.5 Hz producing almost illegible profiles at frequencies close and higher than 1 Hz. The noisy strain profiles were generated by a phase shift between the measured interference data and the baseline data. Thus, limiting the dynamic measuring capacity of the sensing system and therefore its utilization in non-static operational environment. One of the main challenges to be overcome by this type of technology is the inherent noise level observed in the measurement for dynamic testing conditions.

However, the appearance of noise didn't affect the posterior usage of the sensor as observed in final set of fatigue and static test. Thus, it is possible to consider this type of OF system to monitor the performance of the structure after a determined number of flights in static and quasi-static loading conditions.

Although with the current state of art it is already possible to use Fiber Bragg Grating with multiple gratings on a single fiber, the use of Rayleigh backscattering presents an interesting use of commercial off the shelf fibers with no additional post-requirements for strain and temperature measurements. However, the DSS interrogator is still heavy and bulky, requiring further miniaturization and development for implementations in the UAV industry.

Conclusions

An Optic Fiber Distributed Sensing System using the Rayleigh backscattering was proven to be feasible and reliable for composite structures load monitoring applications under static or very low frequency applications (up to 0.5 Hz). The OF measurements were verified with strain gauges obtaining good results at different locations of the structure at the corresponding load levels. The increase in the amount of data collected with respect to previous sensors implies considerable advantages in terms of in lab testing and FEM verifications. The results of the research have a big potential in the case of the UAV field in order to increase the load spectrum knowledge of those vehicles and to determine the structural integrity of primary structures. Moreover, the integrated sensor allows carrying out further FEM verifications by comparing model results and distributed sensing measurements of the instrumented structure. Thus, improving thereby the behavior prediction capacity of the FE model that may lead to Digital Twin Formulation for Aerospace Structures.

The primary limitation observed in this study for the application of a Rayleigh backscattering system for in-flight load monitoring is the dynamic response. Unacceptable noise levels were observed for loading frequencies above 0.5 Hz. The response of small structures, typical of UAVs will experience loading spectrums with higher frequencies. Thus, improvement in this capability will be required in the future for widespread acceptance of this technology.

Acknowledgments

The authors would like to acknowledge the funding received through the FP7 Marie Curie Career Integration Grant titled: Monitoring of Aerospace Structural Shapes (MASS) (Grant no. 618316) and the Erasmus Research Grant from Universidad Politécnica de Madrid. Special thanks to Mr. Johan Bonder, Mr. Fred Bosh, Mr. Misha Huizinga, Mr. Gerjan and Mr. Bart Wiegant from the Structural Integrity and Composites group at Delft University of Technology, for their technical support on this study.

References

- [1] G. E. Muller, C. J. Schmid, Factor of Safety – USAF Design Practice, Report Number: AFFDL-TR-78-8, September (1977)
- [2] SAE –Aerospace Recommended Practices – Guidelines for Implementation of Structural Health Monitoring of Fixed Wing Aircraft ARP6461
- [3] M.A. Hamid, M. Abdullah-Al-Wadud, M. M. Alam, A reliable structural health monitoring protocol using wireless sensor networks, 14th International Conference on Computer and Information Technology - ICCIT, (2011) pp.601,606, 22-24, doi: 10.1109/ICCITech.2011.6164859
- [4] R. F. Guratzsch, S. Mahadevan, Structural Health Monitoring Sensor Placement Optimization Under Uncertainty, AIAA Journal, Vol. 48, No. 7, (2010) pp. 1281-1289
- [5] C. Mandache, M. Genest, M. Khan, N. Mrad, Considerations on Structural Health Monitoring Reliability, International Workshop on Smart Materials, Structures & NDT in

- Aerospace, Montreal, Province of Quebec, Canada, 2-4th of November 2011.
- [6] C. M. S. Kabban, B. M. Greenwell, M. P. DeSimio, M. M. Derriso, The probability of detection for structural health monitoring systems: Repeated measures data Structural Health Monitoring, *Journal of Structural Health Monitoring*, January 29, 2015, doi:10.1177/1475921714566530
 - [7] J. Dodson, D. Inman, Thermal sensitivity of Lamb waves for structural health monitoring applications, *Journal of Ultrasonic*, (2013) pp. 677-685.
 - [8] N. Gandhi, J. E. Michaels, S. J. Lee., Acoustoelastic Lamb wave propagation in bi-axially stressed plate, *Journal Acoustical Society America*, (2012) pp. 1284-1293.
 - [9] M.J.G.N. Boon, D. Zarouchas, M. Martinez, D. Gagar, R. Benedictus, P. Foote, Temperature and load effects on acoustic emission signals for structural health monitoring applications, *Proceedings of EWSHM-7th European Workshop on Structural Health Monitoring*, 2014.
 - [10] Chris, R. s.l., The outlook for unmanned aircraft, *High Performance Composites*, (2009) Vol. May 2009.
 - [11] T.Aldag, A. Crockett, J. Tomblin, *Airframe Technology Assessment of the Airworthiness of Unmanned Aerial Systems*, Daytona Beach: FAA Center of Excellence for General Aviation Research, 2009.
 - [12] *Load Spectrum Development for Unmanned Aerial Systems Airworthiness*. Daytona Beach: FAA Centre of Excellence for General Aviation Research, 2010.
 - [13] W. Staszewski, C. Boller, G. Tomlinson, *Health Monitoring of Aerospace Structures, Smart Sensors Technologis and Signal Processing*. s.l., Wiley, 2003.
 - [14] R.M. s.l. Measures, *Smart Composite Structures with Embedded Sensors*, *Composites Engineering*, Vol. 2., (1992).
 - [15] N. D. W. Glossop, *An embedden Optic fiber sensor for Impact Damage Detection in Composite Material*. PhD Thesis, University of Toronto, 1989.
 - [16] D. Loken, *Effect of Fiber straightness on Fatigue of Aligned Continuous CFRP Composites*, Master Thesis. University of Toronto, 1990.
 - [17] S.S. Roberts, R. Davinson. s.l.; *Mechanical Properties of Composite Materials Containing embedded Optic fiber Sensor* SPIE, 1991.
 - [18] C. Keulen, B. Rocha, M. Yildiz, A. Suleman, Embedded fiber optic sensors for monitoring processing, quality and structural health of resin transfer molded components, *Journal of Physics: Conference Series* 305 (2011) 012135, doi:10.1088/1742-6596/305/1/012135
 - [19] P. Beukema. s.l, *Embedding Technologies of FBG Sensors in Composites: Tecnologies, Applications and Practical Use*, 6th European Workshop on Structural Health Monitoring, Tu.4.C.4.
 - [20] E. Udd, S. Kreger, S. Calvert, M. Kunzler, T. Taylor; *Nondestructive Evaluation of Composite Materials Using Multi-axis Fiber Grating Strain Sensors*, Orlando, Blue Road Research, Vol. 5278, 2003.
 - [21] K. Peters, P. Pattis, J. Botsis, P.Giacconi Lausanne, Experimental verification of response of embedded optical fiber Bragg grating sensors in non-homogeneous strain fields, *Optics and Lasers in Engineering*, 2000.
 - [22] C. E. Davis, W. G. A. Brown, P. R. Stoddart. s.l., Temperature-independent Bragg grating based sensor for monitoring regions of localised strain concentration, SPIE, 2009.
 - [23] Huai H. Kee, Gareth P. Lees, and Trevor P. Newson, All-fiber system for simultaneous interrogation of distributed strain and temperature sensing by spontaneous Brillouin scattering, Vol. 25, No. 10, *Optics Letters*, May 15, 2000.
 - [24] O. Frazão, C. Correia, J. L. Santos, J. M. Baptista, Raman fiber Bragg-grating laser sensor with cooperative Rayleigh scattering for strain–temperature measurement, *Meas. Sci. Technol.* 20, 045203 (5pp). 2009.

- [25] D. Samieck, Distributed Fiber Optic Strain and Temperature Measurement with Extremely High Spatial Resolution, 2012.
- [26] R.G. Duncana, B. A. Childersa, V.Rajendranb, High spatial-resolution temperature monitoring of an industrial motor using a distributed fiber-optic sensing technique, SPIE, Vol. 5384, New York, 2013.
- [27] Load Spectrum Development for Unmanned Aerial Systems Airworthiness. Daytona Beach: FAA Centre of Excellence for General Aviation Research, 2010.
- [28] Solar Powered Amphibious Unmanned Aerial Vehicle. Final Report Design and Synthesis Excercise: Faculty of Aerospace Engineering of the Tecnichal University of Delft, 2012/2013.
- [29] P. B. Martinez, Structural Design, FEM Analysis and Manufacturing of a Composite Optic fiber Instrumented UAV Wing, M.Sc. Thesis, Faculty of Aerospace Engineering, Delft University of Technology, Netherlands, 2014.
- [30] A. K. Green, d E. Shafir. s.l., Termination and connection methods for Optical fibers Embedded in Aerospace Composite Componets, Smart Materials and Structures, Vol. 8., 1999.
- [31] J. Bussieres, M. Martinez, D. Barazanchy, D. Debruyne, P. Lava, Load Monitoring using a Rayleigh Backscattering Fiber Optic System, International conference of Adapative Structures and Technologies, Aruba, 2013.
- [32] S. P. Timoshenko, D. H. Young. Theory of Structures. s.l. : McGraw-Hill, 1965